

## High-Throughput Screening of Strong Electron–Phonon Couplings in Ternary Metal Diborides

Renhai Wang, Yang Sun,\* Feng Zhang, Feng Zheng, Yimei Fang, Shunqing Wu, Huafeng Dong,\* Cai-Zhuang Wang, Vladimir Antropov, and Kai-Ming Ho



Cite This: <https://doi.org/10.1021/acs.inorgchem.2c02829>



Read Online

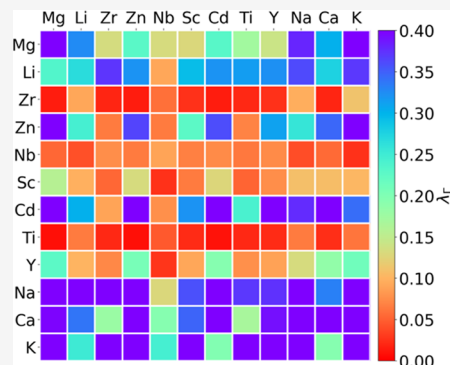
ACCESS |

Metrics & More

Article Recommendations

Supporting Information

**ABSTRACT:** We perform a high-throughput screening on phonon-mediated superconductivity in a ternary metal diboride structure with alkali, alkaline earth, and transition metals. We find 17 ground states and 78 low-energy metastable phases. From fast calculations of zone-center electron–phonon coupling, 43 compounds are revealed to show electron–phonon coupling strength higher than that of MgB<sub>2</sub>. An anticorrelation between the energetic stability and electron–phonon coupling strength is identified. We suggest two phases, i.e., Li<sub>3</sub>ZrB<sub>8</sub> and Ca<sub>3</sub>YB<sub>8</sub>, to be synthesized, which show reasonable energetic stability and superconducting critical temperature.



### 1. INTRODUCTION

Superconductivity has irreplaceable applications in many fields such as energy, medical care, transportation, and quantum computing. The search for new superconductors with a high critical temperature ( $T_c$ ) is always a major scientific task that can open the door to many future techniques. Since 2001, the discovery of a remarkably high superconducting  $T_c$  in MgB<sub>2</sub><sup>1</sup> has stimulated great interest in searching for phonon-mediated superconductors in layered hexagonal metal diboride structures.<sup>2–9</sup> Many attempts have been made to increase the  $T_c$  of MgB<sub>2</sub> by doping other elements,<sup>10–12</sup> which include Mg<sub>1-x</sub>Li<sub>x</sub>B<sub>2</sub>,<sup>13</sup> Mg<sub>1-x</sub>Zr<sub>x</sub>B<sub>2</sub>,<sup>14</sup> Mg<sub>1-x</sub>Zn<sub>x</sub>B<sub>2</sub>,<sup>15</sup> Mg<sub>1-x</sub>Nb<sub>x</sub>B<sub>2</sub>,<sup>16</sup> Mg<sub>1-x</sub>Sc<sub>x</sub>B<sub>2</sub>,<sup>17</sup> Mg<sub>1-x</sub>Ti<sub>x</sub>B<sub>2</sub>,<sup>18</sup> Mg<sub>1-x</sub>Na<sub>x</sub>B<sub>2</sub>,<sup>15</sup> and Mg<sub>1-x</sub>Ca<sub>x</sub>B<sub>2</sub>.<sup>15</sup> However, most experimental data show a decreasing trend of  $T_c$  with an increasing amount of the doping metal. Other metal diboride phases without Mg have also been explored, such as ZrB<sub>2</sub>,<sup>19</sup> NbB<sub>2</sub>,<sup>20</sup> and TaB<sub>2</sub>,<sup>21</sup> however, they only showed a vanishing  $T_c$ . Recent experiments identify MoB<sub>2</sub><sup>22</sup> and WB<sub>2</sub><sup>23</sup> showing a high  $T_c$  while high pressures of greater than 50 GPa are required. First-principle calculations also demonstrated a few possibilities of high  $T_c$  in metal diborides. A well-known case is CaB<sub>2</sub>,<sup>24</sup> where the electron–phonon coupling (EPC) is much stronger than that in MgB<sub>2</sub>. Unfortunately, it is difficult to synthesize due to inferior thermodynamic stability. Doping with Cd and Ba in MgB<sub>2</sub> is predicted to show higher  $T_c$  than MgB<sub>2</sub> but such doped structures are also difficult to be synthesized experimentally.<sup>25,26</sup> Therefore, the thermodynamic stability and superconducting properties should be considered simulta-

neously to find new experimentally feasible ternary superconductors in metal diborides.

While the dopants should be as diverse as possible, it is difficult to efficiently screen out promising superconductors among a large number of candidates with theoretical  $T_c$  calculations. This is mainly because the detailed calculation of the electron–phonon coupling from density functional perturbation theory (DFPT)<sup>27</sup> is complicated and time-consuming. We recently found that single-cell frozen-phonon calculations of the EPC strength of the zone-center phonons can be an efficient alternative to full density functional theory (DFT) evaluation of the Eliashberg function.<sup>28</sup> It well distinguishes strong EPC in MgB<sub>2</sub> and high-pressure hydride systems.<sup>28</sup> Therefore, it can be a fast descriptor of the full Brillouin-zone EPC constant for the metal diboride family. In this work, we employ this method to perform a fast screening of strong EPC on ternary metal diboride phases. A large number of substituted phases are screened based on energetical stability and zone-center EPC strength. The detailed full Brillouin-zone calculations of EPC and  $T_c$  are performed for promising candidates.

Received: August 7, 2022

## 2. COMPUTATIONAL METHODS

The AlB<sub>2</sub>-type primitive cell (space group: *P6/mmm*) was expanded by  $1 \times 1 \times 2$  or  $2 \times 2 \times 1$  to generate M<sub>1-x</sub>N<sub>x</sub>B<sub>2</sub> ternary metal diboride structures (M and N representing the metal elements). The ratio  $\alpha$  includes 0.25 (M<sub>3</sub>NB<sub>8</sub>), 0.50 (MNB<sub>4</sub>), and 0.75 (MN<sub>3</sub>B<sub>8</sub>). Within the limited cell size, we select all symmetry-inequivalent structures from the candidates, which generate one configuration for M<sub>3</sub>NB<sub>8</sub> or MN<sub>3</sub>B<sub>8</sub> and two for MNB<sub>4</sub> (see Supporting Materials Figure S1 for details). The ternary structures were optimized by ab initio calculations, which were performed using the projector augmented wave (PAW) method<sup>29</sup> within density functional theory as implemented in the VASP code.<sup>30,31</sup> The exchange and correlation energy are treated without the spin-polarized generalized gradient approximation (GGA) and parameterized by the Perdew–Burke–Ernzerhof formula (PBE).<sup>32</sup> A plane-wave basis was used with a kinetic energy cutoff of 520 eV, and the convergence criterion for the total energy was set to  $10^{-5}$  eV. Monkhorst–Pack's sampling scheme<sup>33</sup> was adopted for Brillouin-zone sampling with a *k*-point grid of  $2\pi \times 0.033 \text{ \AA}^{-1}$ . The lattice vectors (supercell shape and size) and atomic coordinates are fully relaxed until the force on each atom is less than 0.01 eV/Å.

The formation energy  $E_f$  of ternary M<sub>x</sub>N<sub>y</sub>B<sub>z</sub> is calculated by

$$E_f = \frac{E(M_xN_yB_z) - xE(M) - yE(N) - zE(B)}{x + y + z} \quad (1)$$

where  $E(M_xN_yB_z)$  is the total energy of M<sub>x</sub>N<sub>y</sub>B<sub>z</sub>;  $E(M)$ ,  $E(N)$ , and  $E(B)$  are the total energy of M, N, and B ground-state bulk phases, respectively. To characterize the energetic stability of M<sub>x</sub>N<sub>y</sub>B<sub>z</sub>, we calculated the formation energy differences with respect to the three reference phases, named M<sub>x1</sub>N<sub>y1</sub>B<sub>z1</sub>, M<sub>x2</sub>N<sub>y2</sub>B<sub>z2</sub>, and M<sub>x3</sub>N<sub>y3</sub>B<sub>z3</sub>, forming the Gibbs triangle on the convex hull (denoted as  $E_d$ ). Considering M<sub>x</sub>N<sub>y</sub>B<sub>z</sub>  $\rightarrow$   $\alpha M_{x1}N_{y1}B_{z1} + \beta M_{x2}N_{y2}B_{z2} + \gamma M_{x3}N_{y3}B_{z3}$ ,  $E_d$  can then be calculated as

$$E_d = \frac{E_f(M_xN_yB_z) - \alpha E_f(M_{x1}N_{y1}B_{z1}) - \beta E_f(M_{x2}N_{y2}B_{z2}) - \gamma E_f(M_{x3}N_{y3}B_{z3})}{x + y + z} \quad (2)$$

If  $E_d = 0$ , it indicates that M<sub>x</sub>N<sub>y</sub>B<sub>z</sub> is a new ground state and the existing convex hull should be updated. The reference of convex hulls is obtained from the Materials Project data set.<sup>34</sup>

The high-throughput screening of strong EPC in these metal borides is based on the fast frozen-phonon calculation of the zone-center EPC strength,<sup>28</sup> defined by

$$\lambda_{\Gamma\nu} = \sum_{\nu} \lambda_{\Gamma\nu} \quad (3)$$

where  $\sum_{\nu}$  indicates the summation of all modes at zone-center  $\Gamma$ .  $\lambda_{\Gamma\nu}$  is defined by

$$\lambda_{\Gamma\nu} = \frac{\tilde{\omega}_{\Gamma\nu}^2 - \omega_{\Gamma\nu}^2}{4\omega_{\Gamma\nu}^2} \quad (4)$$

where  $\omega_{\Gamma\nu}$  and  $\tilde{\omega}_{\Gamma\nu}$  are screened and unscreened phonon frequencies of mode  $\nu$  at the zone-center, respectively. The phonon frequencies were calculated with the single-cell and finite displacement methods implemented in the Phonopy code.<sup>35</sup> The displacement amplitude in the frozen-phonon calculations is 0.02 Å. The convergence criterion of the total energy is  $10^{-8}$  eV.

The calculations of full Brillouin-zone EPC constants and the  $T_c$  of MgB<sub>2</sub>, Li<sub>3</sub>ZrB<sub>8</sub>, and Ca<sub>3</sub>YB<sub>8</sub> were performed based on density functional perturbation theory<sup>27</sup> implemented in the Quantum ESPRESSO code.<sup>36–38</sup> We used the ultrasoft pseudopotentials from the GBRV library.<sup>39</sup> After the convergence test, the plane-wave cutoff and the charge density cutoff were chosen to be 60 and 500 Ry, respectively. The reference calculation of the dynamical matrix and EPC matrix elements in MgB<sub>2</sub> is based on the AlB<sub>2</sub>-type primitive cell. Self-consistent field (SCF) calculations were performed with a dense *k*

mesh of  $48 \times 48 \times 48$ , followed by the DFPT calculation with the *k* mesh of  $24 \times 24 \times 24$  and the *q* mesh of  $6 \times 6 \times 6$ . The calculations of Li<sub>3</sub>ZrB<sub>8</sub> and Ca<sub>3</sub>YB<sub>8</sub> were based on the  $2 \times 2 \times 1$  supercell, using a dense *k* mesh of  $24 \times 24 \times 48$  for the SCF calculation and the *k* mesh of  $12 \times 12 \times 24$  and the *q* mesh of  $3 \times 3 \times 6$  for DFPT calculations. The convergence threshold in DFPT calculations was  $1 \times 10^{-12}$  Ry. The Gaussian smearing of the width was 0.01 Ry.

The isotropic Eliashberg spectral function was obtained via the average over the Brillouin zone<sup>40</sup>

$$\alpha^2(\omega)F(\omega) = \frac{1}{2N(\epsilon_F)} \sum_{qv} \frac{\gamma_{qv}}{\hbar\omega_{qv}} \delta(\omega - \omega_{qv}) \quad (5)$$

where  $N(\epsilon_F)$  is the density of states at the Fermi level  $\epsilon_F$ ;  $\omega_{qv}$  denotes the phonon frequency of mode  $\nu$  with wave vector  $q$ .  $\gamma_{qv}$  is the phonon linewidth defined by  $\gamma_{qv} = \frac{2\pi\alpha_{qv}}{\Omega_{BZ}} \sum_{ij} \int d^3k |g_{k,qv}^{ij}|^2 \delta(\epsilon_{q,i} - \epsilon_F) \delta(\epsilon_{k+q,j} - \epsilon_F)$ , where  $g_{k,qv}^{ij}$  is the EPC matrix element;  $\epsilon_{q,i}$  and  $\epsilon_{k+q,j}$  are eigenvalues of Kohn–Sham orbitals at bands  $i, j$ , and wave vectors  $q, k$ . The full Brillouin-zone EPC constant  $\lambda$  is determined through the integration of the Eliashberg spectral function

$$\lambda = 2 \int \frac{\alpha^2(\omega)F(\omega)}{\omega} d\omega \quad (6)$$

The  $T_c$  is obtained with the analytical McMillan equation<sup>41</sup> modified by Allen–Dynes<sup>42,43</sup>

$$T_c = \frac{\omega_{\log}}{1.2} \exp \left[ \frac{-1.04(1 + \lambda)}{\lambda(1 - 0.62\mu^*) - \mu^*} \right] \quad (7)$$

where  $\omega_{\log}$  is the logarithmic average frequency  $\omega_{\log} = \exp[\frac{2}{\lambda} \int \frac{d\omega}{\omega} \alpha^2(\omega)F(\omega)\log\omega]$  and  $\mu^*$  is the effectively screened Coulomb repulsion constant, set as 0.1. While the estimation of  $T_c$  is done using a “single band” approach for this work, it is well known that the superconductivity in MgB<sub>2</sub> has a multiband character.<sup>3,9</sup> A corresponding multiband modification of the McMillan formula can be applied with ref 9. We leave these calculations of multiband superconductivity for the future.

## 3. RESULTS AND DISCUSSION

**3.1. Binary Metal Diboride Phases.** We first examine the effect of metal substitution in the binary metal diboride structure with 12 elements including Ca, Cd, K, Na, Zn, Li, Nb, Y, Sc, Zr, Ti, and Mg. The energetic stability is described by the energy above the convex hull  $E_d$  (see Section 2 for the definition of  $E_d$ ). The EPC strength is described with the zone-center EPC strength  $\lambda_{\Gamma}$  (see Section 2 for the definition of  $\lambda_{\Gamma}$ ). As shown in Figure 1, Zr, Ti, Sc, Y, and Nb diborides show

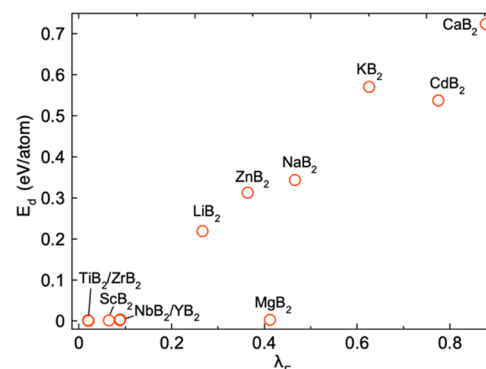


**Figure 1.**  $E_d$ – $\lambda_{\Gamma}$  diagram of 12 binary MB<sub>2</sub> structures. Lower  $E_d$  indicates better stability. Higher  $\lambda_{\Gamma}$  indicates stronger EPC.

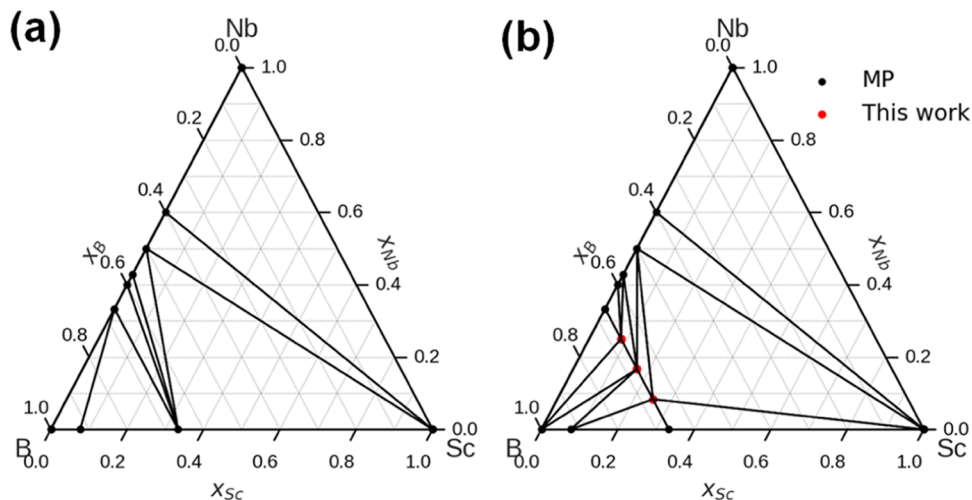


**Figure 2.** Convex hull of the Sc–Nb–B system. (a) Previously reported phases from the MP database and (b) convex hull including the  $\text{ScNbB}_4$ ,  $\text{ScNb}_3\text{B}_8$ , and  $\text{Sc}_3\text{NbB}_8$  phases. Black lines separate the compositional space into Gibbs triangles.

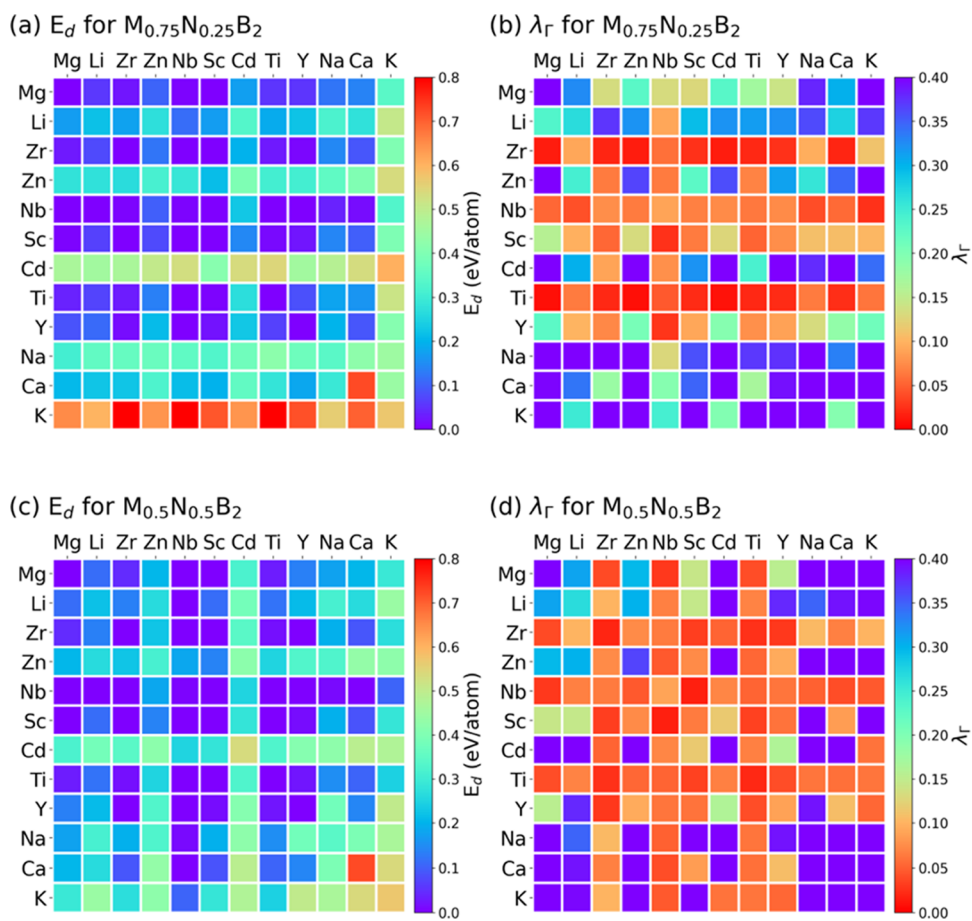


**Figure 3.**  $E_d$  and  $\lambda$  mapping of ternary metal diboride compounds. (a) and (b) are  $E_d$  and  $\lambda$  for  $\text{M}_{0.75}\text{N}_{0.25}\text{B}_2$ ; (c) and (d) are  $E_d$  and  $\lambda$  for  $\text{M}_{0.5}\text{N}_{0.5}\text{B}_2$ . x-axis indicates N site, and y-axis indicates M site.

good energetic stability but no EPC. Ca, Cd, and K diborides show strong EPC but poor energetic stability. Overall, Figure 1 shows an anticorrelation between  $E_d$  and  $\lambda_\Gamma$  that a stronger EPC (larger  $\lambda_\Gamma$ ) leads to worse energetic stability (higher  $E_d$ ). Interestingly, the  $\text{MgB}_2$  phase shows both a decent  $\lambda_\Gamma$  and strong energetic stability, which is an outlier from the general anticorrelation of the two properties. The  $\text{CaB}_2$  system shows the best EPC but poor energetic stability, making it difficult to

synthesize in experiments.<sup>24</sup> Therefore, the correlation in Figure 1 is in line with the previous findings that substitution of Mg in  $\text{MgB}_2$  either leads to lower  $T_c$  or reduced stability. This demonstrates that the  $\lambda_\Gamma$  provides a good description of the EPC strength for metal diboride systems, consistent with a previous comparative study between  $\text{MgB}_2$  and  $\text{AlB}_2$ .<sup>28</sup>

**3.2.  $\text{M}_{1-x}\text{N}_x\text{B}_2$  Ternary Convex Hull.** We calculate the energetic stability and EPC strength in the ternary  $\text{M}_{1-x}\text{N}_x\text{B}_2$

by mixing 12 metals on the metal sites in the supercell of the  $\text{AlB}_2$  structure (see Section 2). The combination of M and N results in 66 ( $C_{12}^2$ ) M–N–B ternary systems with 198 geometrically inequivalent structures containing three compositions, i.e.,  $\text{MNB}_4$ ,  $\text{MN}_3\text{B}_8$ , and  $\text{M}_3\text{NB}_8$ . The convex hull is constructed for each ternary phase to describe its energetic stability. Taking Nb–Sc–B as an example in Figure 2, the compositional space (Gibbs triangle) is partitioned into multiple triangular pieces by the ground-state structures, which form the corners of the convex hull for the corresponding ternary system. The known stable ground states are obtained from the Materials Project (MP)<sup>34</sup> database. In Figure 2a, the known Na–Sc–B phases form a reference convex hull. If any new structure has formation energy below this convex hull surface, it is defined as a new ground state, and the convex hull surface is updated by including the new phase. In Figure 2b, three Na–Sc–B structures ( $\text{ScNbB}_4$ ,  $\text{ScNb}_3\text{B}_8$ ,  $\text{Sc}_3\text{NbB}_8$ ) are found to be the ground-state phases, considerably modifying the original convex hull reference, shown in Figure 2a.

In total, 17 ternary phases are identified as ground states, including  $\text{ScNbB}_4$ ,  $\text{ScNb}_3\text{B}_8$ ,  $\text{Sc}_3\text{NbB}_8$ ,  $\text{LiNb}_3\text{B}_8$ ,  $\text{CaNbB}_4$ ,  $\text{YNbB}_4$ ,  $\text{YZrB}_4$ ,  $\text{ZrScB}_4$ ,  $\text{Zr}_3\text{ScB}_8$ ,  $\text{ZrNbB}_4$ ,  $\text{ScTiB}_4$ ,  $\text{Mg}_3\text{ScB}_8$ ,  $\text{MgNbB}_4$ ,  $\text{MgNb}_3\text{B}_8$ ,  $\text{Ti}_3\text{NbB}_8$ ,  $\text{TiNbB}_4$ , and  $\text{TiNb}_3\text{B}_8$ . Two of them, i.e.,  $\text{TiNbB}_4$  and  $\text{ZrNbB}_4$ , were previously reported in the MP database. Moreover,  $\text{Mg}_{0.75}\text{Sc}_{0.25}\text{B}_2$ <sup>17</sup> and three  $\text{Zr}_{1-x}\text{Nb}_x\text{B}_2$  ( $x = 0.25, 0.5, 0.75$ ) were experimentally synthesized.<sup>44</sup> The convex hulls are updated by including the new ground states, shown in Supporting Materials Figure S2. In addition, we identify many low-energy metastable states that may be synthesizable by experiments, especially under nonequilibrium synthesis routes. For instance, recent experiments on LiNiB showed that the  $\text{Li}_{0.75}[\text{NiB}]_2$  phase with  $E_d = 0.21$  eV/atom can be synthesized from high-temperature reactions.<sup>45</sup> Metastable  $\text{SnTi}_2\text{N}_4$  ( $E_d = 0.2$  eV/atom)<sup>46</sup> and metastable  $\text{ZnMoN}_2$  in a wurtzite-derived structure ( $E_d = 0.16$  eV/atom)<sup>47</sup> are all successfully synthesized in experiments. Here, using a threshold of  $E_d < 0.2$  eV/atom, we identify 78 metastable metal diboride phases, which may have experimental synthesizability. Detailed information on these metastable phases is shown in Supporting Table S1. We note that the present work only considered the  $\text{AlB}_2$  prototypical structure. From the computational point of view, to determine whether structures can be synthesized in practice, other crystal structures may also be considered. A crystal structure search with USPEX,<sup>48</sup> CALYPSO,<sup>49</sup> AGA,<sup>50,51</sup> etc., can be applied to the system of interest in the future.

**3.3.  $E_d$ – $\lambda_\Gamma$  Correlation in Ternary  $\text{M}_{1-x}\text{N}_x\text{B}_2$ .** To describe EPC,  $\lambda_\Gamma$  values are computed for all ternary  $\text{M}_{1-x}\text{N}_x\text{B}_2$ . The maps of  $E_d$  and  $\lambda_\Gamma$  with all substituted structures are shown in Figure 3. The color of each grid indicates the  $E_d$  or  $\lambda$  value of the corresponding phases. The more bluish coding indicates better energetic stability or stronger EPC. The data of the binary phases are listed in the diagonal grids as a reference. One can see that the compounds containing Mg, Zr, Nb, Sc, Ti, and Y elements show better thermodynamic stability, while those containing Mg, Li, Cd, Na, Ca, and K have better EPC strength.

The  $E_d$ – $\lambda_\Gamma$  correlations of all ternary phases are plotted in Figure 4a, which also shows a general trend of the anticorrelation between stability and EPC strength, although the ternary data points appear to be more scattered than the binary ones shown in Figure 1. To understand the cation

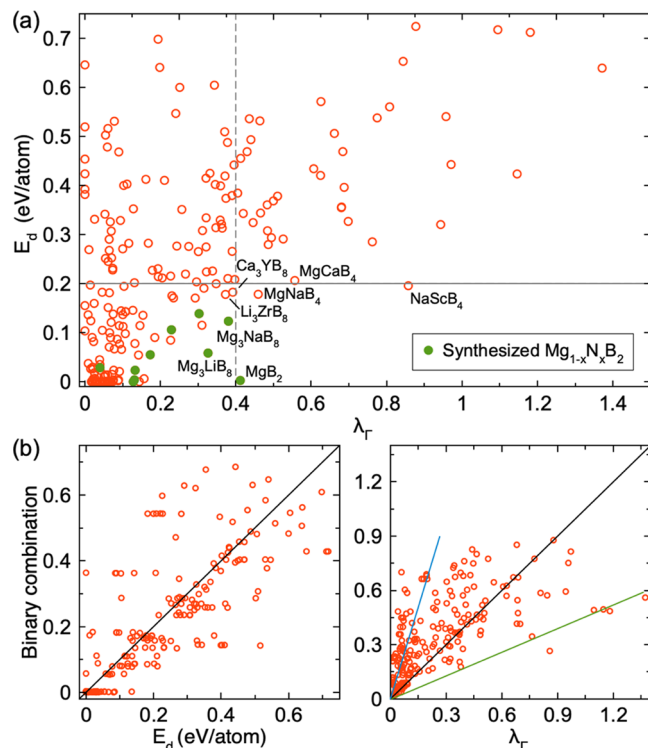


**Figure 4.**  $E_d$  and  $\lambda_\Gamma$  correlation in ternary metal diborides. (a)  $E_d$ – $\lambda_\Gamma$  diagram for ternary  $\text{M}_{1-x}\text{N}_x\text{B}_2$  structures. The green solid symbol indicates phases previously synthesized by experiments.<sup>1,13–18</sup> The horizontal line indicates the range of synthesizable energetic stability. The vertical dashed line indicates the  $\lambda_\Gamma$  value similar to  $\text{MgB}_2$ . (b) Comparison between the  $E_d$  (left panel) and  $\lambda_\Gamma$  (right panel) of ternary phases and the linear combinations of their binary counterparts.  $x$ -axis shows the value of ternary phases, i.e.,  $E_d(\text{M}_{1-x}\text{N}_x\text{B}_2)$  or  $\lambda_\Gamma(\text{M}_{1-x}\text{N}_x\text{B}_2)$ .  $y$ -axis shows the linear combination of the binary counterparts, i.e.,  $(1-x)E_d(\text{MB}_2) + xE_d(\text{NB}_2)$  or  $(1-x)\lambda_\Gamma(\text{MB}_2) + x\lambda_\Gamma(\text{NB}_2)$ . The black line indicates the  $y = x$  correlation. Blue and green lines indicate the weakening and enhancement of  $\lambda_\Gamma$ , respectively.

mixing effect in ternary phases, we recalculate  $E_d$  and  $\lambda_\Gamma$  values by linearly interpolating between binary phases (e.g.,  $E_d(\text{M}_{1-x}\text{N}_x\text{B}_2) = (1-x)E_d(\text{MB}_2) + xE_d(\text{NB}_2)$ ), and compare the interpolated values with the real values in Figure 4b.  $E_d$  mostly follows the  $y = x$  line, indicating insignificant mixing enthalpy for the ternary phases. However,  $\lambda_\Gamma$  in Figure 4b strongly deviates from the  $y = x$  line. A large group of ternary phases show a deteriorated  $\lambda_\Gamma$  compared to the linear combination of parent phases (blue line in Figure 4b). Only a small group of ternary phases show an enhancement of  $\lambda_\Gamma$  due to the mixing (green line). This provides a qualitative explanation to many previously failed attempts at increasing the  $T_c$  of  $\text{MgB}_2$  by doping with other elements because the substitution has a much higher chance of deteriorating, instead of enhancing, the EPC. Therefore, it is necessary to perform high-throughput screening of many substitution possibilities. We also checked the correlation between the density of states at Fermi levels  $N(\epsilon_F)$  and  $E_d$  or  $\lambda_\Gamma$  and verified that  $N(\epsilon_F)$  is not a dominant factor to fully describe the total energy and EPC.

A few ternary metal diborides containing Mg have been successfully synthesized previously,<sup>1,13–18</sup> as marked in Figure 4. Table 1 lists detailed information on the doped  $\text{Mg}_{1-x}\text{N}_x\text{B}_2$  that has been reported experimentally or calculated theoret-

**Table 1. Zone-Center EPC Strength  $\lambda_\Gamma$ , Previously Calculated  $T_c$  or Experimental  $T_c$ , and Energy above the Convex Hull  $E_d$  from Present Calculations for Doped  $Mg_{1-x}N_xB_2$  Phases<sup>a</sup>**

$Mg_{1-x}N_xB_2$	$\lambda_\Gamma$	calculated $T_c$ (K)	experimental $T_c$ (K)	$E_d$ (eV/atom)
$MgB_2$	0.41	42 <sup>26</sup>	39 <sup>1</sup>	0.0
$Mg_{0.75}Nb_{0.25}B_2$	0.13		39.3 ( $x = 0.05$ )	0.004
$Mg_{0.75}Li_{0.25}B_2$	0.33	31 ( $x = 0.2$ )	38.3 ( $x = 0.3$ )	0.058
$Mg_{0.75}Na_{0.25}B_2$	0.38	44–54 ( $x = 0.2$ )	38 ( $x = 0.1$ )	0.123
$Mg_{0.75}Ca_{0.25}B_2$	0.31	41–52 ( $x = 0.2$ )	38 ( $x = 0.1$ )	0.139
$Mg_{0.75}Zn_{0.25}B_2$	0.23	33 ( $x = 0.2$ )	38 ( $x = 0.2$ )	0.106
$Mg_{0.75}Zr_{0.25}B_2$	0.13		37.3 ( $x = 0.2$ )	0.023
$Mg_{0.75}Ti_{0.25}B_2$	0.18	25.5 <sup>25</sup>	30 ( $x = 0.2$ )	0.055
$Mg_{0.75}Sc_{0.25}B_2$	0.13	11.4 <sup>25</sup>	8.2 <sup>17</sup>	0.0
$Mg_{0.5}Ti_{0.5}B_2$	0.04	4.9 <sup>25</sup>	26 ( $x = 0.4$ )	0.029
$Mg_{0.5}Sc_{0.5}B_2$	0.15	8.8 <sup>25</sup>		0.003

<sup>a</sup>The  $x$  in the bracket shows the previously studied composition.

ically.<sup>1,13–18,25,52,53</sup> One can see that  $\lambda_\Gamma$  shows a consistent trend with the reported  $T_c$  values, indicating that the zone-center EPC calculation can reliably estimate the superconducting properties of this material family. It is important to note that experiments show that 20% of Zn, 10% of Na, and 10% of Ca can be doped in the  $MgB_2$  structure,<sup>15</sup> while their  $E_d$  values are in the range of 0.1–0.2 eV/atom. Therefore, it provides a range of  $E_d$  to identify metastable phases that may be accessible in experiments. In Figure 4, we use  $E_d < 0.2$  eV/atom as the criteria to select structures with good stability. We use a threshold of  $\lambda_\Gamma \sim 0.4$ , (i.e.,  $\lambda_\Gamma$  of  $MgB_2$ ) to screen out structures with good EPC. The phases of interest that satisfy both criteria are located in the lower-right area of Figure 4a.

While most phases in or near this area are the doped  $MgB_2$ , it also identifies three non- $MgB_2$  phases for further study, namely,  $NaScB_4$ ,  $Li_3ZrB_8$ , and  $Ca_3YB_8$ . By checking the full Brillouin-zone phonon spectrum, we find that  $NaScB_4$  shows strong imaginary phonons (see Supporting Figure S3), while  $Li_3ZrB_8$  and  $Ca_3YB_8$  are dynamically stable. By analyzing the zone-center phonon modes, we find that the EPCs in both systems are contributed by Raman-active  $E_{2g}$  modes, as shown in Figure S4. These modes are two-dimensional on the boron layers, similar to the stretching modes in  $MgB_2$ , while the distributions on boron atoms are different (Figure S4). It is interesting to note that  $\lambda_\Gamma$  of  $Li_3ZrB_8$  is higher than those of  $LiB_2$  and  $ZrB_2$ . Therefore,  $Li_3ZrB_8$  can be an example of the enhanced EPC group due to the mixing (green line in Figure 4b).

**3.4. Superconductivity in  $Li_3ZrB_8$  and  $Ca_3YB_8$ .** Because of the promising synthesizability and EPC in  $Li_3ZrB_8$  and  $Ca_3YB_8$  phases, we perform DFPT calculations to compute the full Brillouin zone EPC constant and calculate  $T_c$  with McMillan equations (see Section 2). Figure 5 shows the electronic structure and phonon spectrum for  $Li_3ZrB_8$ . The bands at the Fermi level are mainly from B's  $p$  electrons mixed with Zr's  $d$  electrons (Figure 5a). Compared to the electronic structure of  $MgB_2$  (Supporting Figure S5), the flat bands from  $\Gamma$  to A show a cross at the Fermi level, which also results in a significant change in the Fermi surface in Figure 5b.

The phonon spectrum and density of states of  $Li_3ZrB_8$  are shown in Figure 5c. No imaginary frequency modes are identified along the Brillouin zone's high-symmetry lines, indicating that  $Li_3ZrB_8$  is dynamically stable. Three twofold degenerate  $E_{2g}$  modes of B atoms show strong EPC at the  $\Gamma$  point. This is consistent with the frozen-phonon analysis,

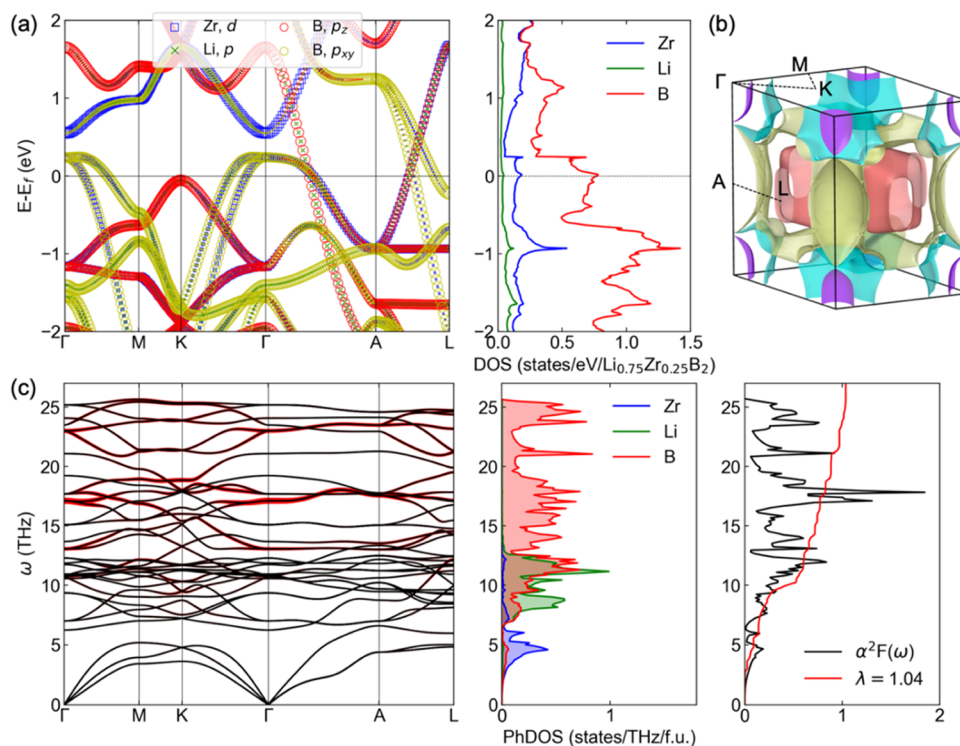


**Figure 5. Electron structure and electron–phonon calculations for  $Li_3ZrB_8$ .** (a) Electronic band structure and projected density of states. (b) Fermi surface. (c) Phonon dispersion, phonon density of state, and Eliashberg spectrum. The red bands on the phonon dispersion indicate the strength of EPC.

shown in Figure 5. Unlike  $\text{MgB}_2$  that the  $E_{2g}$  mode only shows EPC along the  $\Gamma$ –A line (Supporting Figure S5), the  $E_{2g}$  modes in  $\text{Li}_3\text{ZrB}_8$  show EPC more evenly distributed in the Brillouin zone. This leads to an EPC constant  $\lambda = 1.04$ , much higher than the value of 0.62 for  $\text{MgB}_2$  in the present calculation. The electronic and phonon analyses are also performed for  $\text{Ca}_3\text{YB}_8$ , as shown in Supporting Figure S6. The  $E_{2g}$  mode of  $\text{Ca}_3\text{YB}_8$  shows EPC only along the  $\Gamma$ –A line, similar to  $\text{MgB}_2$ . The EPC constant of  $\text{Ca}_3\text{YB}_8$  is  $\lambda = 0.64$ .

We calculate  $T_c$  for  $\text{Li}_3\text{ZrB}_8$  and  $\text{Ca}_3\text{YB}_8$  with McMillan equations. We also recalculate  $T_c$  for  $\text{MgB}_2$  with the same method and the same density of  $k$ - and  $q$ -grids (see Section 2). This provides us a reference to estimate  $T_c$  in the two ternary systems. For  $\text{MgB}_2$ , we obtain isotropic  $T_c = 19$  K with the Allen–Dynes formula. This is consistent with the previous calculation (22 K in ref 6) but underestimates the  $T_c$  compared to the experimental value of 39 K. The error is mainly due to the McMillan equation. One can improve it by employing a more sophisticated anisotropic Eliashberg theory<sup>24</sup> and the Migdal–Eliashberg equation.<sup>54</sup> The nonadiabatic effects, which have been shown to be significant for  $\text{MgB}_2$  and related systems,<sup>55–57</sup> may also be considered for ternary metal borides in future studies. Nevertheless, using the same accuracy, we obtain  $T_c$  as 38 and 10 K for  $\text{Li}_3\text{ZrB}_8$  and  $\text{Ca}_3\text{YB}_8$ , respectively. Therefore, the application of the McMillan formula for  $\text{Li}_3\text{ZrB}_8$  produced  $T_c$  almost twice as large as the one in  $\text{MgB}_2$ , while the  $T_c$  of  $\text{Ca}_3\text{YB}_8$  is half of  $\text{MgB}_2$ .

## 4. CONCLUSIONS

In summary, using first-principles high-throughput calculations, we search for ternary metal diborides with energetic stability and high EPC strength in 66 systems; 17 phases are identified to be stable ternary ground states, and the ternary phase diagrams of these systems are updated accordingly; 78 metastable phases with  $E_d < 0.2$  eV/atom are also identified. An anticorrelation between the energetic stability and EPC strength is revealed in both binary and ternary metal diborides. Two systems,  $\text{Li}_3\text{ZrB}_8$  and  $\text{Ca}_3\text{YB}_8$ , show both good energetic stability and strong EPC strength. The  $T_c$  of  $\text{Li}_3\text{ZrB}_8$  is predicted to be twice as large as that of  $\text{MgB}_2$ , calculated based on the McMillan formalism with the same parameters. The experimental verification of our prediction is highly desirable. Our studies demonstrate zone-center phonon calculations as an encouraging method for the massive screening of multi-component systems for conventional high- $T_c$  superconductors.

## ■ ASSOCIATED CONTENT

### SI Supporting Information

The Supporting Information is available free of charge at <https://pubs.acs.org/doi/10.1021/acs.inorgchem.2c02829>.

Crystal structures (Figure S1); convex hull (Figure S2); phonon dispersion of  $\text{NaScB}_4$  (Figure S3); zone-center phonon and EPC for  $\text{Li}_3\text{ZrB}_8$  and  $\text{Ca}_3\text{YB}_8$  (Figure S4); electron structure and electron–phonon calculations for  $\text{MgB}_2$  and  $\text{Ca}_3\text{YB}_8$  (Figures S5 and S6); and energy data for low-energy ternary phases (Table S1) ([PDF](#))

## ■ AUTHOR INFORMATION

### Corresponding Authors

Yang Sun – Department of Physics, Iowa State University, Ames, Iowa 50011, United States; Department of Applied Physics and Applied Mathematics, Columbia University, New

York, New York 10027, United States; [orcid.org/0000-0002-4344-2920](https://orcid.org/0000-0002-4344-2920); Email: [yangsun@iastate.edu](mailto:yangsun@iastate.edu)

Huafeng Dong – School of Physics and Optoelectronic Engineering, Guangdong University of Technology, Guangzhou 510006, China; Email: [hfdong@gdut.edu.cn](mailto:hfdong@gdut.edu.cn)

### Authors

Renhai Wang – School of Physics and Optoelectronic Engineering, Guangdong University of Technology, Guangzhou 510006, China

Feng Zhang – Department of Physics, Iowa State University, Ames, Iowa 50011, United States; Ames Laboratory, U.S. Department of Energy, Ames, Iowa 50011, United States

Feng Zheng – Department of Physics, Xiamen University, Xiamen 361005, China

Yimei Fang – Department of Physics, Xiamen University, Xiamen 361005, China

Shunqing Wu – Department of Physics, Xiamen University, Xiamen 361005, China; [orcid.org/0000-0002-2545-0054](https://orcid.org/0000-0002-2545-0054)

Cai-Zhuang Wang – Department of Physics, Iowa State University, Ames, Iowa 50011, United States; Ames Laboratory, U.S. Department of Energy, Ames, Iowa 50011, United States; [orcid.org/0000-0002-0269-4785](https://orcid.org/0000-0002-0269-4785)

Vladimir Antropov – Department of Physics, Iowa State University, Ames, Iowa 50011, United States; Ames Laboratory, U.S. Department of Energy, Ames, Iowa 50011, United States

Kai-Ming Ho – Department of Physics, Iowa State University, Ames, Iowa 50011, United States

Complete contact information is available at:

<https://pubs.acs.org/10.1021/acs.inorgchem.2c02829>

### Notes

The authors declare no competing financial interest.

## ■ ACKNOWLEDGMENTS

R.W. was supported by the Guangdong Basic and Applied Basic Research Foundation (Grant Nos. 2021A1515110328 & 2022A1515012174). Work at the Guangdong University of Technology was supported by the Guangdong Natural Science Foundation of China (Grant Nos. 2017B030306003 and 2019B1515120078). F.Z., Y.F., and S.W. were supported by the National Natural Science Foundation of China (11874307). C.-Z.W., V.A., and F.Z. were supported by the U.S. Department of Energy (DOE), Office of Science, Basic Energy Sciences, Materials Science and Engineering Division. Ames Laboratory is operated for the U.S. DOE by Iowa State University under Contract No. DE-AC02-07CH11358, including the grant of computer time at the National Energy Research Supercomputing Center (NERSC) in Berkeley. Y.S. was supported by the National Science Foundation Award No. DMR-2132666. R.W. and H.D. also thank the Center of Campus Network and Modern Educational Technology of GDUT for providing computational resources and technical support for this work.

## ■ REFERENCES

- (1) Nagamatsu, J.; Nakagawa, N.; Muranaka, T.; Zenitani, Y.; Akimitsu, J. Superconductivity at 39 K in Magnesium Diboride. *Nature* **2001**, *410*, 63–64.
- (2) Buzea, C.; Yamashita, T. Review of the Superconducting Properties of  $\text{MgB}_2$ . *Supercond. Sci. Technol.* **2001**, *14*, R115.

- (3) Kortus, J.; Mazin, I. I.; Belashchenko, K. D.; Antropov, V. P.; Boyer, L. L. Superconductivity of Metallic Boron in MgB<sub>2</sub>. *Phys. Rev. Lett.* **2001**, *86*, 4656–4659.
- (4) Belashchenko, K. D.; Schilfgaarde, Mv.; Antropov, V. P. Coexistence of Covalent and Metallic Bonding in the Boron Intercalation Superconductor MgB<sub>2</sub>. *Phys. Rev. B* **2001**, *64*, No. 092503.
- (5) An, J. M.; Pickett, W. Superconductivity of MgB<sub>2</sub>: Covalent Bonds Driven Metallic. *Phys. Rev. Lett.* **2001**, *86*, 4366.
- (6) Liu, A. Y.; Mazin, I. I.; Kortus, J. Beyond Eliashberg Superconductivity in MgB<sub>2</sub>: Anharmonicity, Two-Phonon Scattering, and Multiple Gaps. *Phys. Rev. Lett.* **2001**, *87*, No. 087005.
- (7) Kong, Y.; Dolgov, O.; Jepsen, O.; Andersen, O. Electron-Phonon Interaction in the Normal and Superconducting States of MgB<sub>2</sub>. *Phys. Rev. B* **2001**, *64*, No. 020501.
- (8) Choi, H. J.; Roundy, D.; Sun, H.; Cohen, M. L.; Louie, S. G. First-Principles Calculation of the Superconducting Transition in MgB<sub>2</sub> within the Anisotropic Eliashberg Formalism. *Phys. Rev. B* **2002**, *66*, No. 020513.
- (9) Mazin, I. I.; Antropov, V. P. Electronic Structure, Electron-Phonon Coupling, and Multiband Effects in MgB<sub>2</sub>. *Phys. C* **2003**, *385*, 49–65.
- (10) Cava, R. J.; Zandbergen, H. W.; Inumaru, K. The Substitutional Chemistry of MgB<sub>2</sub>. *Phys. C* **2003**, *385*, 8–15.
- (11) Karpinski, J.; Zhigadlo, N. D.; Katrych, S.; Puzniak, R.; Rogacki, K.; Gonnelli, R. Single Crystals of MgB<sub>2</sub>: Synthesis, Substitutions and Properties. *Phys. C* **2007**, *456*, 3–13.
- (12) Karpinski, J.; Zhigadlo, N.; Katrych, S.; Rogacki, K.; Batlogg, B.; Tortello, M.; Puzniak, R. MgB<sub>2</sub> Single Crystals Substituted with Li and with Li-C: Structural and Superconducting Properties. *Phys. Rev. B* **2008**, *77*, No. 214507.
- (13) Pallecchi, I.; Brotto, P.; Ferdeghini, C.; Putti, M.; Palenzona, A.; Manfrinetti, P.; Geddo Lehmann, A.; Orecchini, A.; Petrillo, C.; Sacchetti, F.; Affronte, M.; Allodi, G.; De Renzi, R.; Serventi, S.; Andreone, A.; Lamura, G.; Daghero, D.; Gonnelli, R. S.; Tortello, M. Investigation of Li-Doped MgB<sub>2</sub>. *Supercond. Sci. Technol.* **2009**, *22*, No. 095014.
- (14) Feng, Y.; Zhao, Y.; Pradhan, A. K.; Cheng, C. H.; Yau, J. K. F.; Zhou, L.; Koshizuka, N.; Murakami, M. Enhanced Flux Pinning in Zr-Doped MgB<sub>2</sub> Bulk Superconductors Prepared at Ambient Pressure. *J. Appl. Phys.* **2002**, *92*, 2614–2619.
- (15) Toulemonde, P.; Musolino, N.; Flükiger, R. High-Pressure Synthesis of Pure and Doped Superconducting MgB<sub>2</sub> Compounds. *Supercond. Sci. Technol.* **2003**, *16*, 231.
- (16) Kalavathi, S.; Divakar, C. Superconductivity in Dense Mg<sub>11-x</sub>M<sub>x</sub>B<sub>2</sub> (M = Zr, Nb, Mo; x = 0.05) Materials Sintered under Pressure. *Bull. Mater. Sci.* **2005**, *28*, 249–252.
- (17) Agrestini, S.; Metallo, C.; Filippi, M.; Simonelli, L.; Campi, G.; Sanipoli, C.; Liarokapis, E.; De Negri, S.; Giovannini, M.; Saccone, A.; et al. Substitution of Sc for Mg in MgB<sub>2</sub>: Effects on Transition Temperature and Kohn Anomaly. *Phys. Rev. B* **2004**, *70*, No. 134514.
- (18) Lee, B. W.; Choi, I.; Jung, C. U.; Lee, S. I. Doping in MgB<sub>2</sub> Superconductors Using a High-Pressure Furnace. *J. Magn. Magn. Mater.* **2008**, *320*, e484–e486.
- (19) Gasparov, V. A.; Sidorov, N.; Zver'Kova, I.; Kulakov, M. Electron Transport in Diborides: Observation of Superconductivity in ZrB<sub>2</sub>. *J. Exp. Theor. Phys. Lett.* **2001**, *73*, 532–535.
- (20) Leyarovska, L.; Leyarovski, E. A Search for Superconductivity Below 1 K in Transition Metal Borides. *J. Less-Common Met.* **1979**, *67*, 249–255.
- (21) Rosner, H.; Pickett, W.; Drechsler, S.-L.; Handstein, A.; Behr, G.; Fuchs, G.; Nenkov, K.; Müller, K.-H.; Eschrig, H. Electronic Structure and Weak Electron-Phonon Coupling in TaB<sub>2</sub>. *Phys. Rev. B* **2001**, *64*, No. 144516.
- (22) Pei, C.; Zhang, J.; Wang, Q.; Zhao, Y.; Gao, L.; Gong, C.; Tian, S.; Luo, R.; Lu, Z.-Y.; Lei, H. Pressure-Induced Superconductivity at 32 K in MoB<sub>2</sub>. 2021, arXiv preprint arXiv:2105.13250. arXiv.org e-Print archive. <https://arxiv.org/abs/2105.13250>.
- (23) Lim, J.; Hire, A. C.; Quan, Y.; Kim, J. S.; Xie, S. R.; Sinha, S.; Kumar, R. S.; Popov, D.; Park, C.; Hemley, R. J.; Hamlin, J. J.; Hennig, R. G.; Hirschfeld, P. J.; Stewart, G. R. Creating Superconductivity in WB<sub>2</sub> through Pressure-Induced Metastable Planar Defects. 2021, arXiv preprint arXiv:2109.11521. arXiv.org e-Print archive. <https://arxiv.org/abs/2109.11521>.
- (24) Choi, H. J.; Louie, S. G.; Cohen, M. L. Prediction of Superconducting Properties of CaB<sub>2</sub> Using Anisotropic Eliashberg Theory. *Phys. Rev. B* **2009**, *80*, No. 064503.
- (25) Mackinnon, I. D. R.; Talbot, P. C.; Alarco, J. A. Phonon Dispersion Anomalies and Superconductivity in Metal Substituted MgB<sub>2</sub>. *Comput. Mater. Sci.* **2017**, *130*, 191–203.
- (26) Alarco, J. A.; Talbot, P. C.; Mackinnon, I. D. Phonon Anomalies Predict Superconducting T<sub>c</sub> for AlB<sub>2</sub>-Type Structures. *Phys. Chem. Chem. Phys.* **2015**, *17*, 25090–25099.
- (27) Baroni, S.; de Gironcoli, S.; Dal Corso, A.; Giannozzi, P. Phonons and Related Crystal Properties from Density-Functional Perturbation Theory. *Rev. Mod. Phys.* **2001**, *73*, 515–562.
- (28) Sun, Y.; Zhang, F.; Wang, C.-Z.; Ho, K.-M.; Mazin, I. I.; Antropov, V. Electron-Phonon Coupling Strength from ab initio Frozen-Phonon Approach. *Phys. Rev. Mater.* **2022**, *6*, No. 074801.
- (29) Blöchl, P. E. Projector Augmented-Wave Method. *Phys. Rev. B* **1994**, *50*, 17953–17979.
- (30) Kresse, G.; Furthmüller, J. Efficiency of Ab-Initio Total Energy Calculations for Metals and Semiconductors Using a Plane-Wave Basis Set. *Comput. Mater. Sci.* **1996**, *6*, 15–50.
- (31) Kresse, G.; Furthmüller, J. Efficient Iterative Schemes for ab initio Total-Energy Calculations Using a Plane-Wave Basis Set. *Phys. Rev. B* **1996**, *54*, 11169–11186.
- (32) Perdew, J. P.; Burke, K.; Ernzerhof, M. Generalized Gradient Approximation Made Simple. *Phys. Rev. Lett.* **1996**, *77*, 3865–3868.
- (33) Monkhorst, H. J.; Pack, J. D. Special Points for Brillouin-Zone Integrations. *Phys. Rev. B* **1976**, *13*, 5188–5192.
- (34) Jain, A.; Ong, S. P.; Hautier, G.; Chen, W.; Richards, W. D.; Dacek, S.; Cholia, S.; Gunter, D.; Skinner, D.; Ceder, G.; Persson, K. A. Commentary: The Materials Project: A Materials Genome Approach to Accelerating Materials Innovation. *APL Mater.* **2013**, *1*, No. 011002.
- (35) Togo, A.; Tanaka, I. First Principles Phonon Calculations in Materials Science. *Scr. Mater.* **2015**, *108*, 1–5.
- (36) Giannozzi, P.; Baroni, S.; Bonini, N.; Calandra, M.; Car, R.; Cavazzoni, C.; Ceresoli, D.; Chiarotti, G. L.; Cococcioni, M.; Dabo, I.; et al. Quantum Espresso: A Modular and Open-Source Software Project for Quantum Simulations of Materials. *J. Phys.: Condens. Matter* **2009**, *21*, No. 395502.
- (37) Giannozzi, P.; Andreussi, O.; Brumme, T.; Bunau, O.; Nardelli, M. B.; Calandra, M.; Car, R.; Cavazzoni, C.; Ceresoli, D.; Cococcioni, M.; et al. Advanced Capabilities for Materials Modelling with Quantum Espresso. *J. Phys.: Condens. Matter* **2017**, *29*, No. 465901.
- (38) Giannozzi, P.; Baseggio, O.; Bonfa, P.; Brunato, D.; Car, R.; Carnimeo, I.; Cavazzoni, C.; de Gironcoli, S.; Delugas, P.; Ferrari Ruffino, F.; Ferretti, A.; Marzari, N.; Timrov, I.; Ururu, A.; Baroni, S. Quantum Espresso toward the Exascale. *J. Chem. Phys.* **2020**, *152*, No. 154105.
- (39) Garrity, K. F.; Bennett, J. W.; Rabe, K. M.; Vanderbilt, D. Pseudopotentials for High-Throughput DFT Calculations. *Comput. Mater. Sci.* **2014**, *81*, 446–452.
- (40) Eliashberg, G. Interactions between Electrons and Lattice Vibrations in a Superconductor. *Sov. Phys. JETP* **1960**, *11*, 696–702.
- (41) McMillan, W. L. Transition Temperature of Strong-Coupled Superconductors. *Phys. Rev.* **1968**, *167*, 331.
- (42) Allen, P. B. Neutron Spectroscopy of Superconductors. *Phys. Rev. B* **1972**, *6*, No. 2577.
- (43) Allen, P. B.; Dynes, R. Transition Temperature of Strong-Coupled Superconductors Reanalyzed. *Phys. Rev. B* **1975**, *12*, No. 905.
- (44) Akarsu, M. K.; Akin, I. Effects of Graphene Nanoplatelets and Hexagonal Boron Nitride on Spark Plasma Sintered (Zr,Nb)B<sub>2</sub> Solid Solutions. *J. Alloys Compd.* **2021**, *884*, No. 161110.

- (45) Bhaskar, G.; Gvozdetskyi, V.; Batuk, M.; Wiaderek, K. M.; Sun, Y.; Wang, R.; Zhang, C.; Carnahan, S. L.; Wu, X.; Ribeiro, R. A.; et al. Topochemical Deintercalation of Li from Layered LiNiB: Toward 2D MBene. *J. Am. Chem. Soc.* **2021**, *143*, 4213–4223.
- (46) Bikowski, A.; Siol, S.; Gu, J.; Holder, A.; Mangum, J. S.; Gorman, B.; Tumas, W.; Lany, S.; Zakutayev, A. Design of Metastable Tin Titanium Nitride Semiconductor Alloys. *Chem. Mater.* **2017**, *29*, 6511–6517.
- (47) Arca, E.; Lany, S.; Perkins, J. D.; Bartel, C.; Mangum, J.; Sun, W.; Holder, A.; Ceder, G.; Gorman, B.; Teeter, G.; Tumas, W.; Zakutayev, A. Redox-Mediated Stabilization in Zinc Molybdenum Nitrides. *J. Am. Chem. Soc.* **2018**, *140*, 4293–4301.
- (48) Oganov, A. R.; Glass, C. W. Crystal Structure Prediction Using ab initio Evolutionary Techniques: Principles and Applications. *J. Chem. Phys.* **2006**, *124*, No. 244704.
- (49) Wang, Y.; Lv, J.; Zhu, L.; Ma, Y. Crystal Structure Prediction Via Particle-Swarm Optimization. *Phys. Rev. B* **2010**, *82*, No. 094116.
- (50) Zhao, X.; Nguyen, M. C.; Zhang, W. Y.; Wang, C. Z.; Kramer, M. J.; Sellmyer, D. J.; Li, X. Z.; Zhang, F.; Ke, L. Q.; Antropov, V. P.; Ho, K. M. Exploring the Structural Complexity of Intermetallic Compounds by an Adaptive Genetic Algorithm. *Phys. Rev. Lett.* **2014**, *112*, No. 045502.
- (51) Wu, S. Q.; Ji, M.; Wang, C.-Z.; Nguyen, M. C.; Zhao, X.; Umemoto, K.; Wentzcovitch, R.; Ho, K.-M. An Adaptive Genetic Algorithm for Crystal Structure Prediction. *J. Phys.: Condens. Matter* **2013**, *26*, No. 035402.
- (52) Singh, P. P. Theoretical Study of Superconductivity in MgB<sub>2</sub> and Its Alloys. *Bull. Mater. Sci.* **2003**, *26*, 131–135.
- (53) Neaton, J.; Perali, A. On the Possibility of Superconductivity at Higher Temperatures in Sp-Valent Diborides. 2001, arXiv preprint cond-mat/0104098. arXiv.org e-Print archive. <https://arxiv.org/abs/cond-mat/0104098>.
- (54) Margine, E. R.; Giustino, F. Anisotropic Migdal-Eliashberg Theory Using Wannier Functions. *Phys. Rev. B* **2013**, *87*, No. 024505.
- (55) Alexandrov, A. S. Nonadiabatic Polaronic Superconductivity in MgB<sub>2</sub> and Cuprates. *Phys. C* **2001**, *363*, 231–236.
- (56) Cappelluti, E.; Ciuchi, S.; Grimaldi, C.; Pietronero, L.; Strässler, S. High  $T_c$  Superconductivity in MgB<sub>2</sub> by Nonadiabatic Pairing. *Phys. Rev. Lett.* **2002**, *88*, No. 117003.
- (57) Szczęśniak, D.; Szczęśniak, R. Signatures of Nonadiabatic Superconductivity in Lithium-Decorated Graphene. *Phys. Rev. B* **2019**, *99*, No. 224512.

## Supporting Information

### High-throughput screening of strong electron-phonon couplings in ternary metal diborides

Renhai Wang<sup>1</sup>, Yang Sun<sup>2,3\*</sup>, Feng Zhang<sup>2,4</sup>, Feng Zheng<sup>5</sup>, Yimei Fang<sup>5</sup>, Shunqing Wu<sup>5</sup>, Huafeng Dong<sup>1\*</sup>, Cai-Zhuang Wang<sup>2,4</sup>, Vladimir Antropov<sup>2,4</sup>, and Kai-Ming Ho<sup>2</sup>

<sup>1</sup>*School of Physics and Optoelectronic Engineering, Guangdong University of Technology,  
Guangzhou 510006, China*

<sup>2</sup>*Department of Physics, Iowa State University, Ames, Iowa 50011, USA*

<sup>3</sup>*Department of Applied Physics and Applied Mathematics, Columbia University, New York, NY,  
10027, USA*

<sup>4</sup>*Ames Laboratory, U.S. Department of Energy, Ames, Iowa 50011, USA*

<sup>5</sup>*Department of Physics, Xiamen University, Xiamen 361005, China*

\*Email: yangsun@iastate.edu or hfdong@gdut.edu.cn

## Contents

Figures S1-S6

Table S1

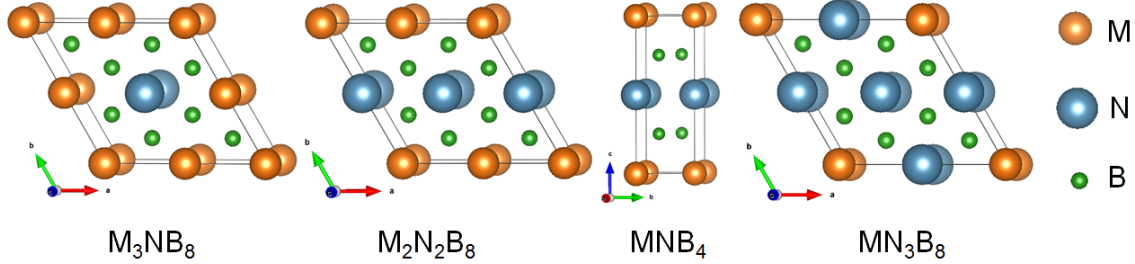


**Figure S1** Four symmetry-inequivalent crystal structures of  $M_3Nb_8$ ,  $MNb_4$  and  $MN_3B_8$ .

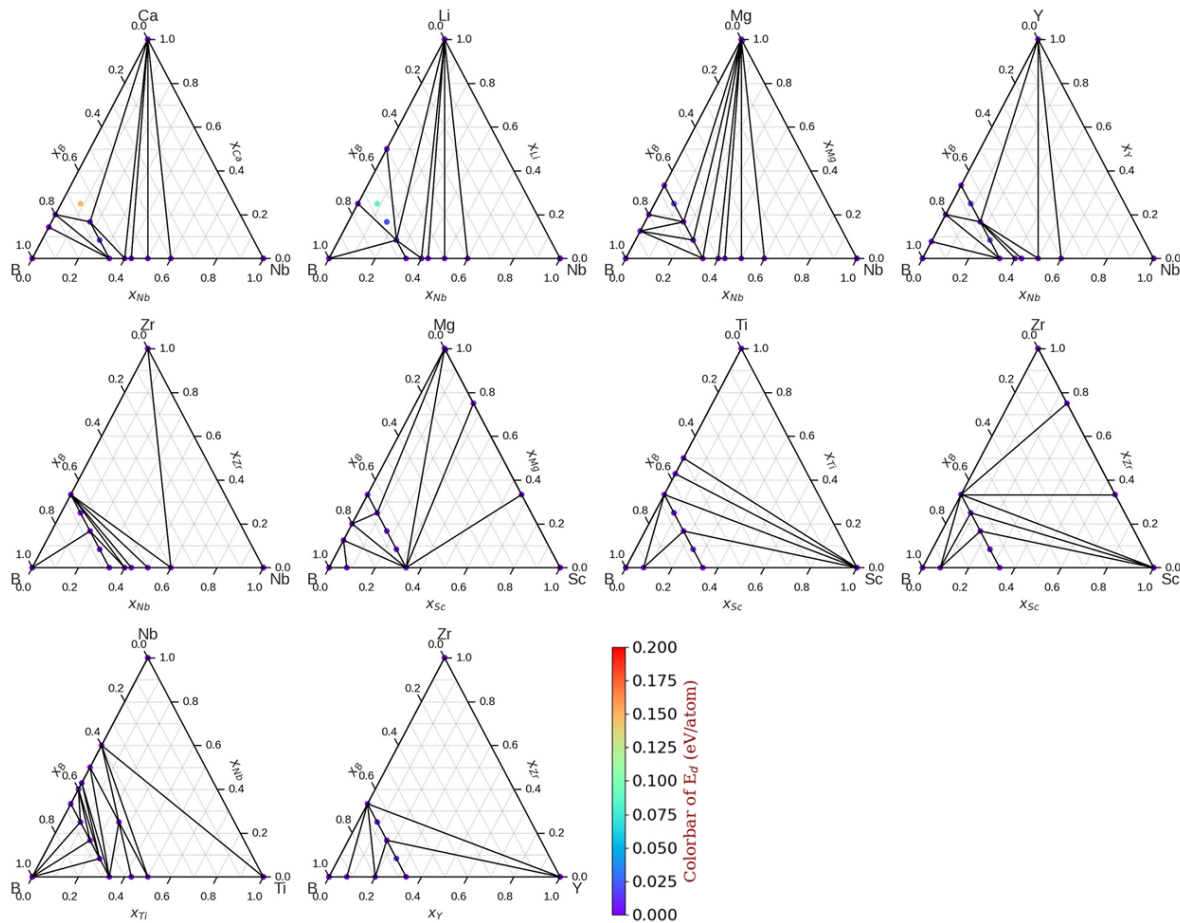


**Figure S2** DFT-calculated convex hull of 10 systems containing ternary ground stable phases. The color bar represents the formation energy above the convex hull ( $E_d$ ).

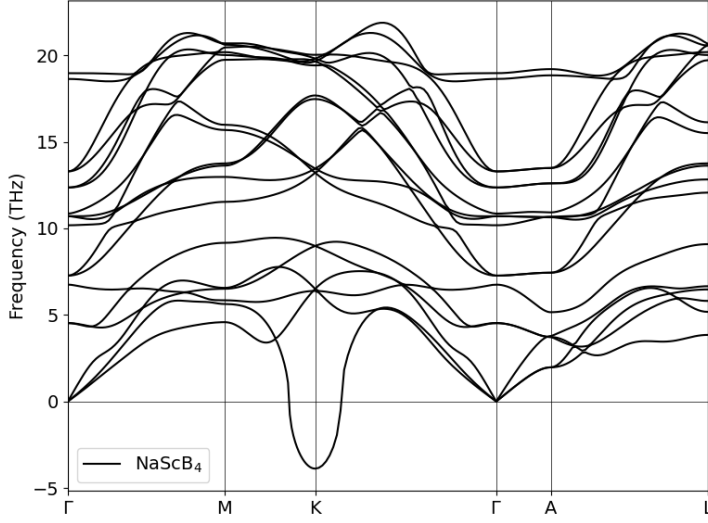


**Figure S3** Phonon dispersion of  $\text{NaScB}_4$ .

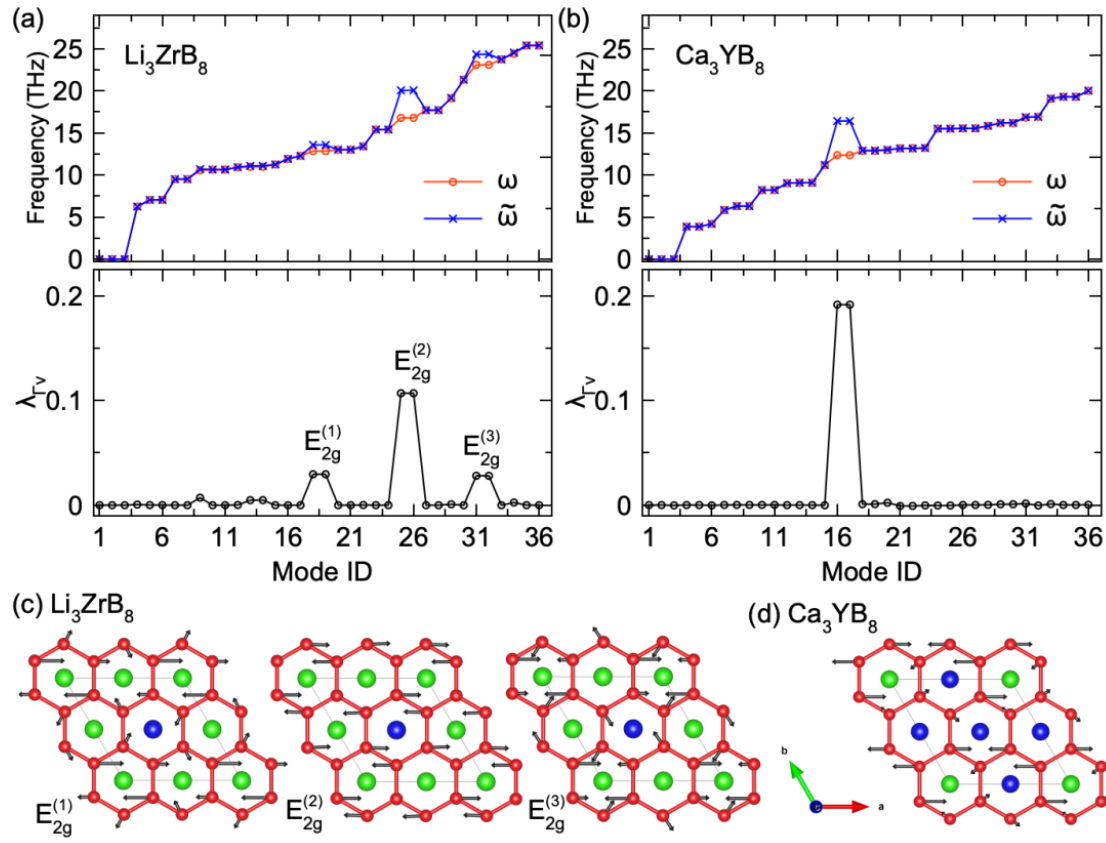


**Figure S4 Analysis of zone-center phonon and EPC from  $\lambda_\Gamma$  calculations.** (a) Upper panel shows the screened and unscreened phonon frequency for zone-center phonon modes for  $\text{Li}_3\text{ZrB}_8$ . Lower panel shows the zone-center EPC strength obtained from Eqn. (3). (b) The phonon frequency and EPC for  $\text{Ca}_3\text{YB}_8$ . (c) and (d) show  $E_{2g}$  modes that contributed to EPC in  $\text{Li}_3\text{ZrB}_8$  and  $\text{Ca}_3\text{YB}_8$ , respectively. Li/Y atoms are colored with green, Zr/Ca atoms are colored with blue and B atoms are colored with red.

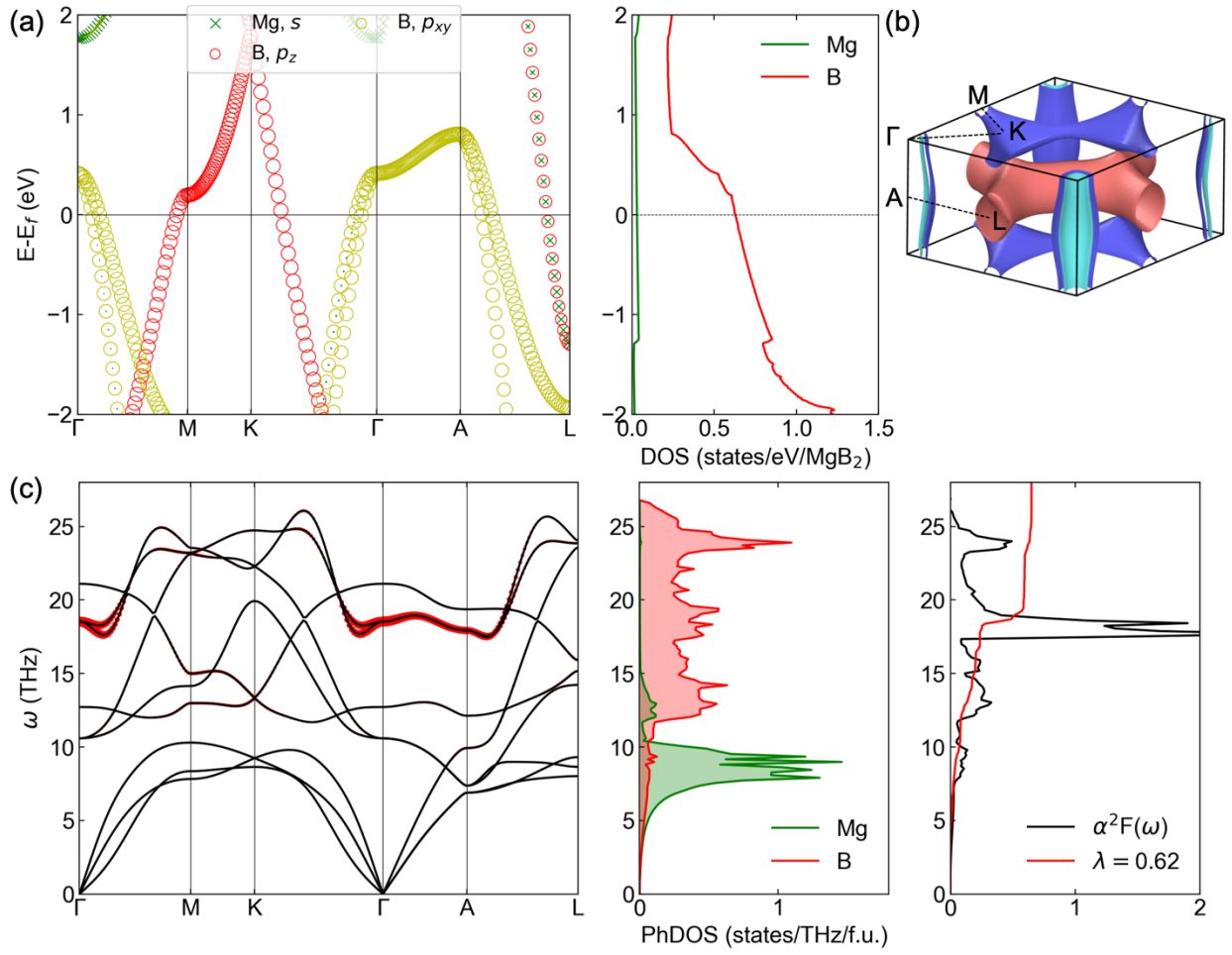


**Figure S5 Electron structure and electron-phonon calculations for  $\text{MgB}_2$ .** (a) Electronic band structure and projected density of states. (b) Fermi surface. (c) Phonon dispersion, phonon density of state and Eliashberg spectrum. The red bands on the phonon dispersion indicates the strength of phonon linewidth.

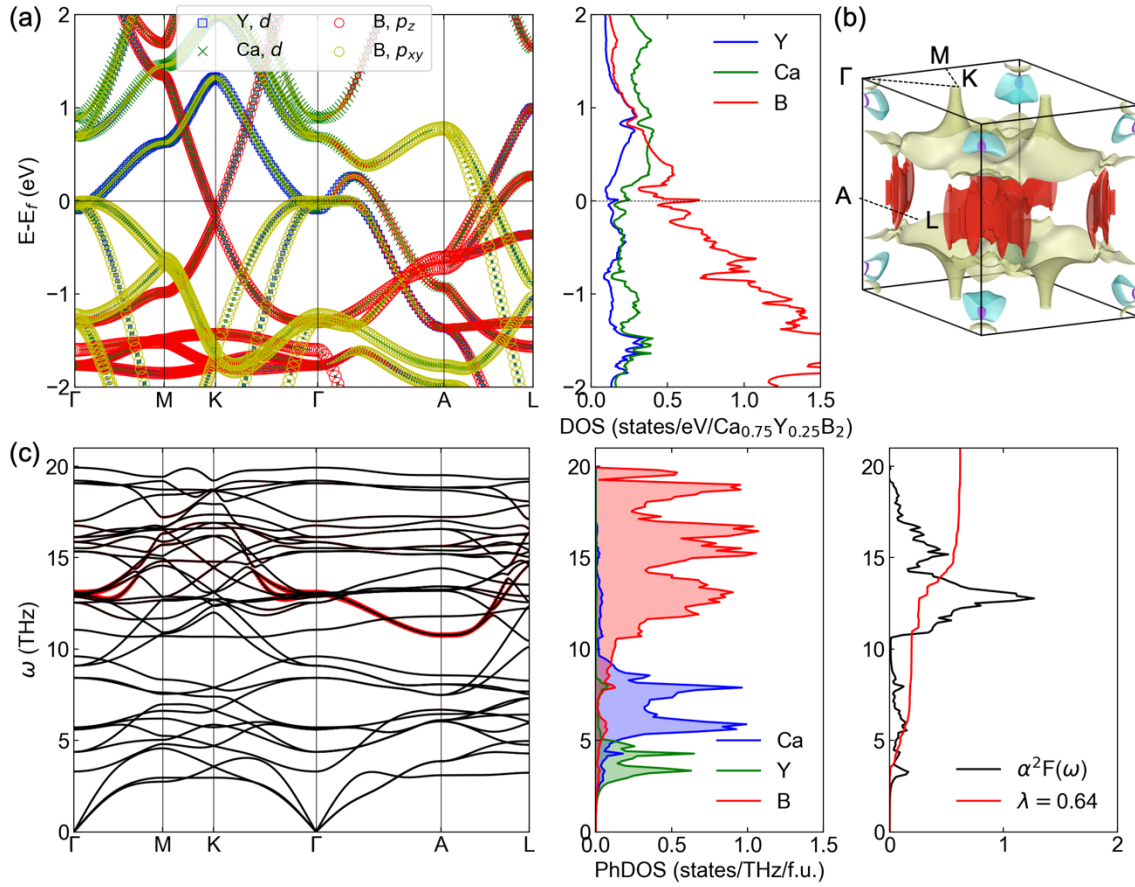


**Figure S6 Electron structure and electron-phonon calculations for  $\text{Ca}_3\text{YB}_8$ .** (a) Electronic band structure and projected density of states. (b) Fermi surface. (c) Phonon dispersion, phonon density of state and Eliashberg spectrum. The red bands on the phonon dispersion indicates the strength of phonon linewidth.

**Table S1** Structure database of ternary compounds which have formation energies within 0.2 eV/atom above the convex hull. The formation energy  $E_f$  (eV/atom) are referenced to pure M, N and B. The energy above convex hull  $E_d$  (eV/atom) are referenced to the stable phases that formed Gibbs triangle. All phases in bold are thermodynamic stable phases and are used to construct the convex hull.

Phases	$E_f$	$E_d$	Phases	$E_f$	$E_d$	Phases	$E_f$	$E_d$
<b>ScNbB<sub>4</sub></b>	<b>-0.907</b>	<b>0</b>	Mg <sub>3</sub> ZrB <sub>8</sub>	-0.334	0.023	LiY <sub>3</sub> B <sub>8</sub>	-0.428	0.112
<b>Sc<sub>3</sub>NbB<sub>8</sub></b>	<b>-0.898</b>	<b>0</b>	YTiB <sub>4</sub>	-0.787	0.023	LiScB <sub>4</sub>	-0.420	0.114
<b>ScNb<sub>3</sub>B<sub>8</sub></b>	<b>-0.834</b>	<b>0</b>	YSc <sub>3</sub> B <sub>8</sub>	-0.760	0.023	LiMgB <sub>4</sub>	-0.081	0.115
<b>YNbB<sub>4</sub></b>	<b>-0.760</b>	<b>0</b>	Zr <sub>3</sub> TiB <sub>8</sub>	-0.997	0.026	LiTiB <sub>4</sub>	-0.508	0.121
<b>MgNbB<sub>4</sub></b>	<b>-0.485</b>	<b>0</b>	MgZr <sub>3</sub> B <sub>8</sub>	-0.771	0.026	NaMg <sub>3</sub> B <sub>8</sub>	-0.004	0.123
<b>MgNb<sub>3</sub>B<sub>8</sub></b>	<b>-0.628</b>	<b>0</b>	Mg <sub>3</sub> NbB <sub>8</sub>	-0.282	0.028	Zr <sub>3</sub> ZnB <sub>8</sub>	-0.639	0.124
<b>LiNb<sub>3</sub>B<sub>8</sub></b>	<b>-0.656</b>	<b>0</b>	MgTiB <sub>4</sub>	-0.560	0.029	Li <sub>3</sub> NbB <sub>8</sub>	-0.232	0.132
<b>CaNbB<sub>4</sub></b>	<b>-0.543</b>	<b>0</b>	ZrTi <sub>3</sub> B <sub>8</sub>	-1.005	0.030	YMgB <sub>4</sub>	-0.365	0.135
<b>ZrScB<sub>4</sub></b>	<b>-0.942</b>	<b>0</b>	LiNbB <sub>4</sub>	-0.480	0.031	Ti <sub>3</sub> ZnB <sub>8</sub>	-0.644	0.136
<b>Zr<sub>3</sub>ScB<sub>8</sub></b>	<b>-0.988</b>	<b>0</b>	YNb <sub>3</sub> B <sub>8</sub>	-0.714	0.033	LiZrB <sub>4</sub>	-0.481	0.137
<b>Mg<sub>3</sub>ScB<sub>8</sub></b>	<b>-0.326</b>	<b>0</b>	NaNb <sub>3</sub> B <sub>8</sub>	-0.528	0.035	ScZnB <sub>4</sub>	-0.292	0.138
<b>Ti<sub>3</sub>NbB<sub>8</sub></b>	<b>-0.977</b>	<b>0</b>	MgTi <sub>3</sub> B <sub>8</sub>	-0.777	0.037	CaMg <sub>3</sub> B <sub>8</sub>	-0.134	0.139
<b>YZrB<sub>4</sub></b>	<b>-0.806</b>	<b>0</b>	MgZrB <sub>4</sub>	-0.533	0.045	CaYB <sub>4</sub>	-0.358	0.142
<b>TiNbB<sub>4</sub></b>	<b>-0.902</b>	<b>0</b>	YMg <sub>3</sub> B <sub>8</sub>	-0.265	0.054	NaSc <sub>3</sub> B <sub>8</sub>	-0.508	0.143
<b>TiNb<sub>3</sub>B<sub>8</sub></b>	<b>-0.819</b>	<b>0</b>	Mg <sub>3</sub> TiB <sub>8</sub>	-0.308	0.055	NaZr <sub>3</sub> B <sub>8</sub>	-0.631	0.144
<b>ZrNbB<sub>4</sub></b>	<b>-0.879</b>	<b>0</b>	LiMg <sub>3</sub> B <sub>8</sub>	-0.108	0.058	Sc <sub>3</sub> CdB <sub>8</sub>	-0.495	0.145
<b>ScTiB<sub>4</sub></b>	<b>-0.945</b>	<b>0</b>	LiSc <sub>3</sub> B <sub>8</sub>	-0.626	0.066	NaTiB <sub>4</sub>	-0.394	0.151
ZrSc <sub>3</sub> B <sub>8</sub>	-0.896	0.000003	Y <sub>3</sub> TiB <sub>8</sub>	-0.629	0.067	CaTi <sub>3</sub> B <sub>8</sub>	-0.702	0.160
Zr <sub>3</sub> NbB <sub>8</sub>	-0.945	0.003	LiTi <sub>3</sub> B <sub>8</sub>	-0.764	0.071	Li <sub>3</sub> ScB <sub>8</sub>	-0.205	0.170
MgScB <sub>4</sub>	-0.497	0.003	LiZr <sub>3</sub> B <sub>8</sub>	-0.740	0.077	Li <sub>3</sub> MgB <sub>8</sub>	-0.048	0.171
ZrNb <sub>3</sub> B <sub>8</sub>	-0.801	0.005	Sc <sub>3</sub> ZnB <sub>8</sub>	-0.562	0.078	Mg <sub>3</sub> CdB <sub>8</sub>	0.041	0.175
ScTi <sub>3</sub> B <sub>8</sub>	-0.987	0.006	YTi <sub>3</sub> B <sub>8</sub>	-0.844	0.082	Li <sub>3</sub> ZrB <sub>8</sub>	-0.240	0.178
YZr <sub>3</sub> B <sub>8</sub>	-0.901	0.008	Y <sub>3</sub> MgB <sub>8</sub>	-0.456	0.084	NaMgB <sub>4</sub>	-0.060	0.178
MgSc <sub>3</sub> B <sub>8</sub>	-0.666	0.010	CaScB <sub>4</sub>	-0.502	0.087	NaTi <sub>3</sub> B <sub>8</sub>	-0.612	0.181
Sc <sub>3</sub> TiB <sub>8</sub>	-0.887	0.011	CaZrB <sub>4</sub>	-0.582	0.090	NbZnB <sub>4</sub>	-0.185	0.182
NaNbB <sub>4</sub>	-0.382	0.011	CaY <sub>3</sub> B <sub>8</sub>	-0.451	0.090	Ca <sub>3</sub> YB <sub>8</sub>	-0.231	0.182
YScB <sub>4</sub>	-0.702	0.014	CaZr <sub>3</sub> B <sub>8</sub>	-0.754	0.097	Li <sub>3</sub> TiB <sub>8</sub>	-0.233	0.190
Y <sub>3</sub> ZrB <sub>8</sub>	-0.675	0.015	CaSc <sub>3</sub> B <sub>8</sub>	-0.621	0.098	NaZrB <sub>4</sub>	-0.340	0.194
ZrTiB <sub>4</sub>	-1.010	0.018	Nb <sub>3</sub> ZnB <sub>8</sub>	-0.451	0.100	NaScB <sub>4</sub>	-0.255	0.196
CaNb <sub>3</sub> B <sub>8</sub>	-0.619	0.020	CaTiB <sub>4</sub>	-0.580	0.103	Zr <sub>3</sub> CdB <sub>8</sub>	-0.566	0.197
Y <sub>3</sub> ScB <sub>8</sub>	-0.628	0.021	KNbB <sub>4</sub>	-0.274	0.105	Ca <sub>3</sub> ScB <sub>8</sub>	-0.258	0.199
Y <sub>3</sub> NbB <sub>8</sub>	-0.647	0.023	Mg <sub>3</sub> ZnB <sub>8</sub>	-0.033	0.106			